

Contents lists available at ScienceDirect

Transportation Research Part B

journal homepage: www.elsevier.com/locate/trb





Optimal investment in driving automation: Individual vs. cooperative sensing

Mehdi Nourinejad a, Sina Bahrami b,*, Yafeng Yin b,c

- ^a Department of Civil and Environmental Engineering, York University, Toronto, Canada
- ^b Department of Civil and Environmental Engineering, University of Michigan, Ann Arbor, United States of America
- c Department of Industrial and Operations Engineering, University of Michigan, Ann Arbor, United States of America

ARTICLE INFO

Keywords: Connected automated vehicles Sensor configuration Cooperative sensing Sensing policy

ABSTRACT

Connected automated vehicles (CAVs) use sensors to scan their surrounding environment in order to make safe and efficient motion decisions. The richness of a CAV's vision depends on the configuration of on-board sensors and the ability of CAVs to share data with nearby vehicles. High-end sensors provide quality data, allowing CAVs to rely on their own sensors through individual sensing, and to become independent of other vehicles. In contrast, sensor data sharing enhances the collective vision of CAVs through cooperative sensing. This study investigates the trade-offs in the values and costs of individual versus cooperative sensing, and it proposes optimal investment strategies for short- and long-term planning. Exploiting the setting of a CAV-exclusive corridor, we propose two nonlinear programs to determine optimal investment in corridor capacity in the long-term, and to maximize social welfare in the short-term through road pricing. Capacity analysis shows disjointed investments in individual and cooperative sensing, first in the former until sensors reach a desired resolution, and then in the latter. Social welfare analysis shows travelers are granted a reward in certain settings, encouraging flows that achieve cooperative sensing. Such rewards are not observed in human-driven vehicle settings that cannot benefit from cooperative sensing.

1. Introduction

Advances in sensing technology and artificial intelligence have expedited the development of connected automated vehicles (CAVs) as an emerging mode of transportation. CAVs use on-board sensors to map a vehicle's surrounding environment for safe and efficient motion decisions. The primary CAV sensors include camera, lidar, and radar. Cameras use highly detailed images to detect, classify, and position objects. Radars emit radio waves that reflect off objects back into a receiver, thus yielding the distance from the vehicle to that object. Lidars use the same principle but emit lasers instead of radio waves. Mounted on a spinner, lidars can generate three-dimensional maps of a vehicle's surroundings. Sensors are broadly assessed in terms of their range and resolution, where range is the threshold distance beyond which a sensor cannot detect objects, and resolution reflects the richness of the sensor data measured in point readings per unit distance (e.g., dots per inch). Fig. 1 depicts the three primary CAV sensors with their range of vision.

The richness of a CAV's vision depends on the configuration of on-board sensors and the ability of CAVs to share data with nearby vehicles. On one hand, high resolution sensors can enhance a CAV's vision, making it autonomous and independent of communicating with other vehicles. On the other hand, when equipped with communications infrastructure such as 5G technology,

E-mail address: sinab@umich.edu (S. Bahrami).

^{*} Corresponding author.

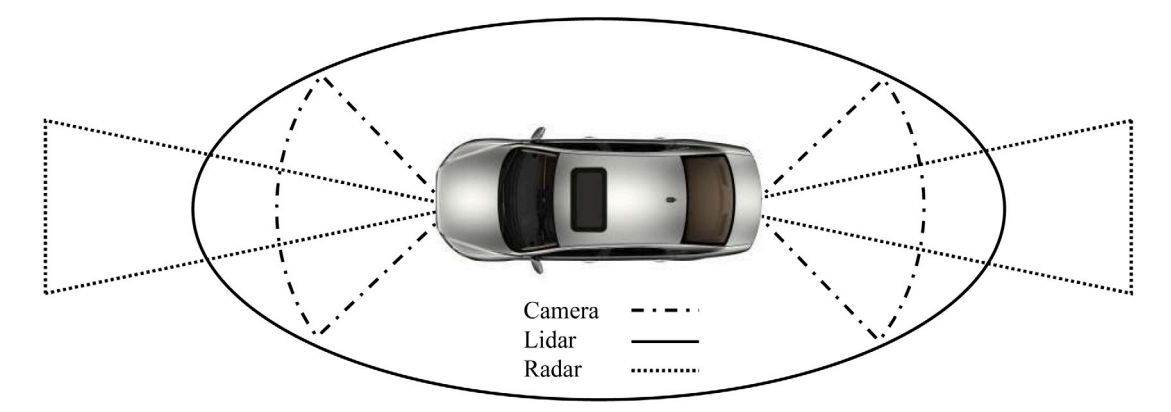


Fig. 1. CAV sensors and their range.

the surrounding vision can be enhanced by sharing sensor data with nearby vehicles. Sensor data sharing can be competitive, complementary, or cooperative. Competitive sensing retrieves data on the same object from multiple sensors, allowing redundancy and higher fault tolerance in detection accuracy (Visser and Groen, 1999). As an example, having more than one radar in front of a CAV improves detection robustness in case any of the radars malfunction. In complementary fusion, sensors do not directly depend on each other, yet their data can be combined to provide a more complete map of the environment, e.g., having multiple cameras pointed at disjunctive areas of a vehicle's surroundings. Cooperative sensing uses independently collected sensor data to infer information otherwise unavailable from any incomplete subset of the sensors. Stereoscopic vision is an example of cooperative sensing that combines two-dimensional images of individual cameras with different viewpoints to generate three-dimensional maps. In the context of this paper, cooperative sensing allows each CAV to use sensor data from the nearby vehicles to broaden its vision. We investigate the trade-offs in the values and costs of individual and cooperative sensing, and propose optimal investment strategies in connectivity and sensor configuration, specifically range and resolution.

Despite growing evidence of the potential benefits of cooperative driving automation (for recent reviews, see Ha et al., 2020 and Labi, 2021), less attention is paid to cooperative sensing, which is related to the role and properties of sensors as the primary source of data shared amongst CAVs. Kianfar et al. (2012) developed and tested a cooperative adaptive cruise control model with sensor data fusion, which uses a Kalman filter to estimate the distance, speed, and acceleration of ego and leader vehicles, considering delays in sensor fusion. Wang et al. (2014a,b) proposed frameworks for adaptive cruise control in platoons for both individual and cooperative control. In the non-cooperative case, each vehicle maximizes driving comfort, efficiency, or safety through optimizing acceleration, speed, or the car following gap using only its leader information accessible by its onboard sensors, while in the cooperative case, all vehicles in the platoon share their state, position, and speed via vehicle-to-vehicle communication. Their analysis shows that cooperative control can outperform individual control as the front vehicles compromise their situations to maximize the benefit of following vehicles in the platoon. Wang et al. (2020) proposed a cooperative adaptive cruise control strategy sensitive to possible communications-related constraints such as interference and information congestion. Their model dynamically optimizes information flow topologies by requiring vehicles to cooperatively determine in real-time their information sending capability. In contrast to all these previous studies, this paper is concerned about societal investment decision on enabling cooperative or individual sensing. Of the most relevant, Vignon et al. (2022) investigated the trade-off between digitalizing infrastructure and equipping vehicles for enabling driving automation. They show that under certain conditions, installing sensors on both infrastructure and vehicles is socially optimal.

This study contributes to understanding optimal social planning policies of individual versus cooperative sensing in automated driving. From a societal point of view, we seek to answer the following questions: (1) If a society can freely decide the investment in enabling cooperative sensing, how it would determine optimal CAV sensor configuration and connectivity level, favoring individual versus cooperative sensing, respectively; (2) what types of investment policies can be implemented in long- and short-term to increase the efficiency of CAVs, and (3) which factors influence investment decisions and to what degree. We assess these policies impacts by developing a stylized model of CAV mobility which is sensitive to the properties of CAV sensors and their ability to share information through cooperative sensing. The framework is leveraged to express average speed and flow in different CAV densities. Our analysis shows that there exists some threshold density beyond which the sensor have enough overlap in their range to facilitate cooperative sensing, thus allowing vehicle to drive at faster speeds due to their longer stretch of vision. Consequently, the travel time function is first constant then decreases with flow due to cooperative sensing effect. When density is further increased, there exists another threshold density beyond which congestion occurs and the average speed drops as is common in the conventional traffic flow of human-driven vehicles. Using the stylized model of CAV mobility, we show that social welfare is maximized when travelers are granted a reward, encouraging higher demand of CAVs to achieve cooperative sensing. Such rewards are not observed in human-driven vehicular flow that cannot benefit from cooperative sensing. Analysis of investing a given budget for maximizing corridor capacity requires disjoint investments in individual and cooperative sensing, first in the former until sensor reach a desire resolution then the latter.

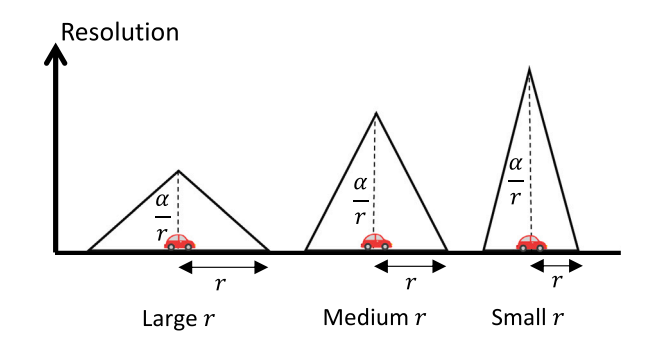


Fig. 2. Sensor range and resolution. The three cases have the same sensor power, but differ in terms of their range and resolution profile.

The rest of this paper is organized as follows: Section 2 presents a stylized model of CAV traffic with sensor configuration and connectivity that is used to assess investment strategies. Section 3 presents the optimal sensor configuration and level of connectivity in long- and short-term investments. Section 4 presents numerical findings on the properties of optimal investment policies. Section 5 presents the conclusions and future research directions.

2. Model

2.1. Sensor range and resolution

Consider a single-lane corridor exclusive to CAVs equipped with sensors to detect the vehicle's surrounding environment. We model the aggregate features of all motion sensors using a single measure of range (how far sensors see) and resolution (how well they see). Sensors only detect objects within a radius r known as range, i.e., each sensor sees a distance r ahead and behind the vehicle. Within their range, sensors better detect objects closer to the vehicle.

We denote the *resolution* of a point located x away from a vehicle by R(x), measured in data points per unit distance (e.g., dpi). Empirical and theoretical studies show that sensor resolution depends on the environment, type of sensor, and distance from objects. Lidar resolution decreases with distance due to the angular deviation of beam channels. Camera resolution is also inversely proportional to its distance with an object, see Figure 7 of Theia Technologies (2022). Equipped with optimally configured sensors, CAVs can attain maximum allowable speeds while abiding by safety protocols. The sensor-oriented traffic flow framework of this study captures traffic properties w.r.t. sensor features, which has been explored less in the relevant literature. Resolution has the following two properties. First, it is well established that $\partial R(x)/\partial x < 0$, indicating that resolution drops with distance between an object and the sensor. Second, sensors have zero resolution on objects beyond their range, therefore R(x) = 0 for x > r.

The assumptions related to sensor resolution are the following (**Assumption 1**): (i) Resolution is symmetric (behind and ahead of the vehicle) as is the case of rotating Lidars. (ii) R(x) is linearly decreasing with x, which satisfies the above resolution properties. (iii) All CAVs have identical resolution profiles.

We define resolution R(x) as

$$R(x) = \frac{\alpha}{r} (1 - \frac{x}{r}) \qquad \forall x \in [0, r], \tag{1}$$

where α is a parameter known as the sensors' *power*, which is the area under R(x) defined as

$$2\int_0^r \frac{\alpha}{r} (1 - \frac{x}{r}) dx = \alpha.$$

Sensor power proportionally increases the resolution at all points within the range as expressed in (1). Lidars and cameras, for example, are often characterized in terms of their vertical and horizontal resolution (and sometimes their angular resolution), the product of which is the number of point receptions per round of reading. Fig. 2 shows a schematic of sensor range and resolution for the same sensor power.

Consider a pair of vehicles on the corridor known as the leader (vehicle moving ahead) and the ego vehicle (vehicle moving behind). Depending on the spacing between the pair, denoted by s, the sensors may achieve no-, partial-, or full-overlap in their range, as shown in Fig. 3. No-overlap occurs when $2r \le s$; partial-overlap occurs when $r \le s < 2r$ where the range of the two sensors overlap, but the vehicles themselves are not within each other's range, and full-overlap occurs when s < r where the vehicles are within each other's range.

The leader can share its sensor data with the ego vehicle, depending on the level of connectivity between the pair. Connectivity is high where there is a faster rate of data exchange or compatibility in fusing the data received from the leader sensor. For example, vehicles from the same manufacturer may be more efficient at sharing sensor information. Vehicle connectivity also depends on the complimentary nature of the data, fusion compatibility (Yeong et al., 2021), and fusion redundancy. Improvements in connectivity can be achieved by investing in communications infrastructure such as LTE and 5G (Campolo et al., 2017), and by standardization of CAV sensors (Zeadally et al., 2020) and data fusion procedures (Hall and Llinas, 2001). Let $\beta \in [0, 1]$ be the connectivity ratio,

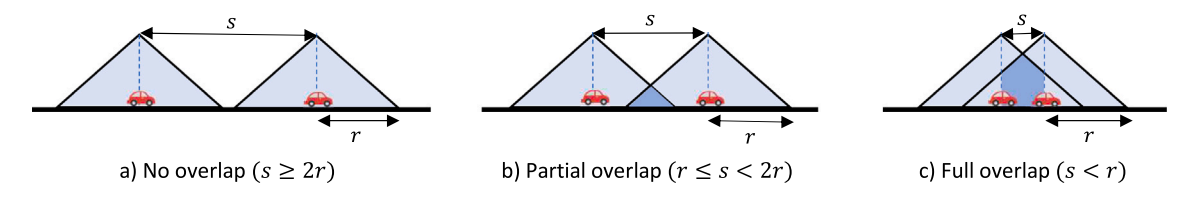


Fig. 3. Sensor range and resolution. The darker color shades indicate a higher resolution.

representing the proportion of data points collected by the leader that is useful and accessible to the ego vehicle. At $\beta=1$ the vehicles are fully connected and have complete access to each other's sensor data, whereas at $\beta=0$ the vehicles are disconnected and cannot share data.

Cooperative sensing allows each CAV to enhance its perceived resolution by relying on its own sensors and the sensors of the vehicle ahead. Let $A(x, \beta, s)$ denote the ego vehicle's augmented resolution at a point located x away from the ego vehicle (in the direction of the leader) given connectivity level β and spacing s. The augmented resolution has the following logical properties prevalent in cooperative sensing:

- *Non-cooperative sensing*: When void of connectivity, i.e., $\beta = 0$, the ego vehicle only has access to its own sensor data and $A(x, \beta, s) = R(x)$, which is independent of the vehicle spacing.
- Augmented resolution bound: The augmented resolution is larger than the individual resolutions of the two sensors within the overlapping stretch of their ranges, i.e., $A(x, \beta, s) \ge \max\{R(x), \beta R(s-x)\}$ for $x \in (\max\{0, s-r\}, \min\{r, s\})$ when s < 2r. Otherwise, cooperative sensing effects are not leveraged if the augmented resolution is smaller than the individual resolution of the sensors.
- Connectivity effects: The augmented resolution increases with connectivity within the overlapping stretch of the sensors' range, i.e., $\frac{\partial A(x,\beta,s)}{\partial \beta} > 0$.

The augmented resolution mapping $A(x, \beta, s)$ has to satisfy the above properties.

The ego vehicle has unrestricted access to its own sensor resolution, R(x), and restricted access to the leader's sensor resolution, R(s-x). Our assumption regarding augmented resolution is that for a given connectivity ratio and spacing between the pair, the ego vehicle receives sensor data from the leader at a resolution of $\beta R(s-x)$. The augmented resolution of the ego vehicle for a point located x away towards the leader is

$$A(x, \beta, s) = R(x) + \beta R(s - x), \tag{2}$$

which represents a weighted augmented resolution function (Rinner and Quaritsch, 2009; Fedorov et al., 2017). Although the communication range is usually larger than the sensor range, it is important to have a resolution of all the distance between two vehicles for setting the vehicles' speeds considering safety concern to ensure that no undetected disturbance exists in traffic. Therefore, the augmented resolution is considered within the spacing between vehicles, s.

We separately specify the augmented resolution in (2) for the three cases of Fig. 3. Let $A_N(x)$, $A_P(x)$, and $A_F(x)$ be the augmented resolutions of the no-, partial-, and full-overlap cases, respectively (we drop β and s for brevity). According to (2), in the no-overlap case

$$A_N(x) = \frac{\alpha}{r} (1 - \frac{x}{r}) \qquad x \le r,\tag{3}$$

in the partial-overlap case,

$$A_{P}(x) = \begin{cases} \frac{\alpha}{r} \left(1 - \frac{x}{r}\right) & x \le s - r \\ \frac{\alpha}{r} \left(1 - \frac{x}{r}\right) + \frac{\alpha\beta}{r} \left(1 - \frac{(s - x)}{r}\right) & s - r < x \le r \\ \frac{\alpha\beta}{r} \left(1 - \frac{(s - x)}{r}\right) & r < x \le s, \end{cases}$$

$$\tag{4}$$

and in the full-overlap case,

$$A_F(x) = \frac{\alpha}{r} \left(1 - \frac{x}{r} \right) + \frac{\alpha \beta}{r} \left(1 - \frac{(s - x)}{r} \right) \qquad x \le s.$$
 (5)

The augmented resolution profiles of the three cases are graphically presented in Fig. 4, which shows that the resolution of the partial-overlap case is discontinuous and non-monotone. We next discuss these properties and their impacts on traffic flow.

2.2. The sight

The sensors surveil a vehicle's surroundings, allowing it to come to a full stop if a disturbance (e.g., object on the road, a jaywalker, or a stopped vehicle) is observed and poses the threat of a crash. We later explain the nature of the disturbances in the derivation of a car-following model in the next subsection for restricted and access-free corridors.

The sensors require an augmented resolution of at least θ , which is a safety threshold parameter, to accurately identify an object and its properties including size, distance (from the vehicle), and speed (Assumption 3). Let T be the sensor's sight (also known as

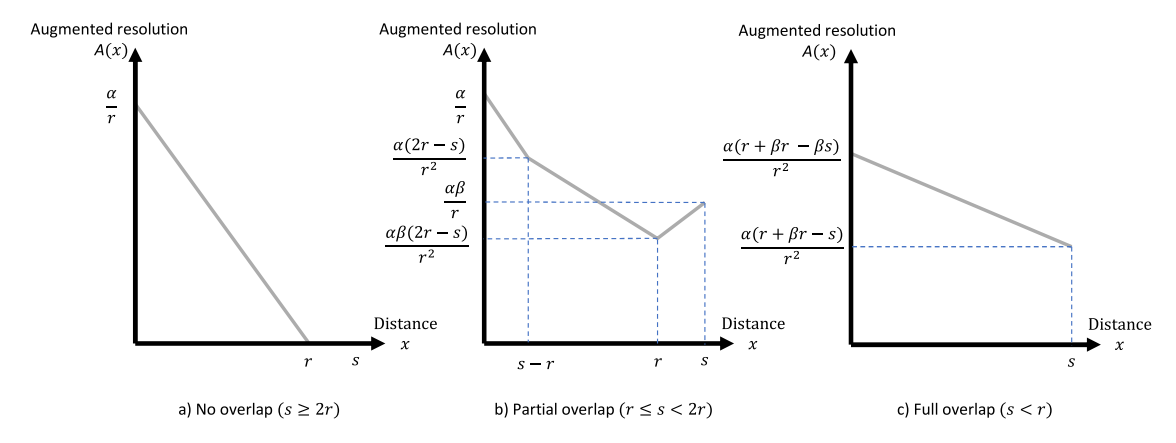


Fig. 4. Augmented resolution of the ego vehicle at a distance of x away in the direction of the leader.

"coverage" in telecommunications), the distance between the ego vehicle and the farthest point that has an augmented resolution of at least θ . The sight is formally defined as

$$T = \max\{x | A(x) \ge \theta\}. \tag{6}$$

According to (6), the largest augmented resolution in the no-overlap case that is achieved at x = 0 and is expressed as $A(0) = \alpha/r$ has to be larger than the safety threshold; otherwise the sensors have no sight. The sensors can accurately detect and classify objects within their sight distance T. For $T < x < \min(s, r)$, the resolution is not sufficient for motion decisions. Note that sight is bounded from above, i.e., $T \le \min(s, r)$, implying that it cannot be larger than the spacing or the range.

Let T_N , T_P , and T_F be the sight of no-overlap ($2r \le s$), partial-overlap ($r \le s < 2r$), and full-overlap (s < r) cases, respectively, which are each a function of the range, safety threshold, spacing, and sensor power.

In the no-overlap case, the sight is

$$T_N = r(1 - \frac{r\theta}{\sigma}),\tag{7}$$

which increases with the sensor power, α , but has a concave behavior w.r.t. range, r. This concave behavior is indicative of the impacts of the range on the sight of the sensors. Thus, a large range is not necessarily ideal if it decreases resolution for a fixed sensor power.

In the partial-overlap case, the sight is

$$T_{P} = \begin{cases} s & r \leq s < 2r - \frac{r^{2}\theta}{a\beta} \\ \frac{(1+\beta)ar - \alpha\beta s - r^{2}\theta}{(1-\beta)a} & 2r - \frac{r^{2}\theta}{a\beta} \leq s < 2r - \frac{r^{2}\theta}{a} \\ r(1 - \frac{r\theta}{a}) & 2r - \frac{r^{2}\theta}{a} \leq s < 2r, \end{cases}$$
(8)

which shows that the sight depends on the range, power, spacing, connectivity, and safety threshold. According to , whenever spacing is higher than a threshold (i.e., $s \ge 2r - \frac{r^2\theta}{a\beta}$), the sight increases with the sensor power and decreases with the safety threshold. In contrast, when the spacing is small (i.e., $s < 2r - \frac{r^2\theta}{a\beta}$), the sight is the same as the spacing, implying that the ego vehicle achieves a resolution larger than θ between itself and the leader vehicle.

In the full-overlap case, the sight is

$$T_F = \begin{cases} s & 0 \le s < r(1+\beta) - \frac{r^2 \theta}{\alpha} \\ \frac{(1+\beta)\alpha r - \alpha\beta s - r^2 \theta}{(1-\beta)\alpha} & r(1+\beta) - \frac{r^2 \theta}{\alpha} \le s < r, \end{cases}$$

$$(9)$$

which exhibits the properties described above.

The sight profile is depicted in Fig. 5, which is continuous, and is sensitive to sensor range and power, connectivity, and safety threshold. The sight initially increases with s as the ego vehicle can oversee the entire stretch between itself and the leader. Sight decreases in medium spacing levels (the thresholds are depicted in the figure) as the pair of vehicles distance themselves from each other and the ego vehicle's sight is shortened. Finally, sight plateaus when spacing is large as the vehicles rely completely on themselves and move in the no-overlap condition.

2.3. Vehicle dynamics

Speed is one of the fundamental variables that capture the state of traffic on the corridor. The allowable traffic speed depends on the sight; vehicles can drive faster if they have a larger sight, making them aware of a larger stretch of the corridor. When notified

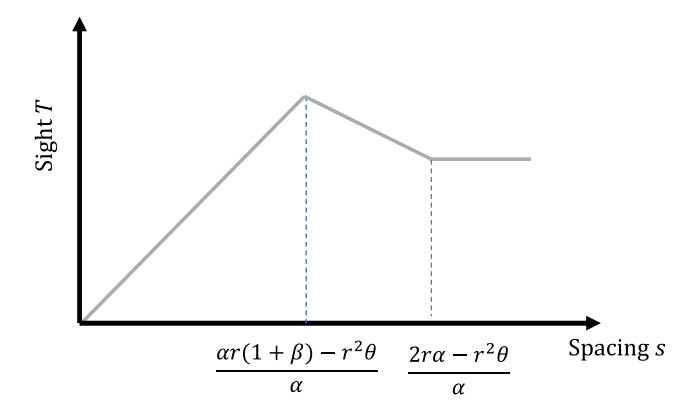


Fig. 5. Sight with respect to vehicle spacing.

of an object (or a disturbance in traffic) at distance T away, the ego vehicle must come to a full stop within a distance T-l, where l is a safety distance, which can be set as the average length of vehicles plus a safety distance between vehicles. This allows vehicles to keep a distance of l with the disturbance when they come to a full stop.

We first focus on restricted access corridors, meaning that the corridor is exclusively used by CAVs driving at the same speed, and there are no stationary objects. An expressway is an example of such corridors. We later extend our analysis to unrestricted access corridors in Appendix A. We denote v as the average speed and define it for these corridors. We also assume that τ is the processing time resembling the time required for the CAVs to observe their environment and make an appropriate motion decision. The processing time is equivalent to the reaction time of regular vehicles. We assume that the reaction times under both individual and cooperative sensing are the same, which is less favorable towards cooperative sensing as this driving strategy can have a lower reaction time due to connectivity properties amongst the vehicles. Considering the same reaction time for both cooperative and individual sensing is rooted in the assumption that only sensor data is shared amongst the vehicles, and they each make individual motion decisions according to the augmented resolution achieved from cooperative sensing.

In restricted corridors, no stand-still objects can suddenly appear on the corridor. Using kinematics, and given that the ego vehicle moves at speed v for τ time units before braking with the same deceleration rate as the leader, we have

$$v = \frac{T - l}{\tau}. ag{10}$$

We express the speed-density relationship as the following. Let k = 1/s be the average vehicle density, which is the inverse of the average spacing between the leader and ego vehicle. Speed for a given density k using Eq. (10) is

$$v = \begin{cases} \frac{r}{\tau} - \frac{r^2 \theta}{\alpha \tau} - \frac{l}{\tau} & k < \frac{\alpha}{2\alpha r - r^2 \theta} \\ \frac{(1+\beta)r}{(1-\beta)\tau} - \frac{r^2 \theta}{(1-\beta)\alpha \tau} - \frac{l}{\tau} - \frac{\beta}{(1-\beta)\tau k} & \frac{\alpha}{2\alpha r - r^2 \theta} \le k < \frac{\alpha}{\alpha r (1+\beta) - r^2 \theta} \\ \frac{1}{\tau k} - \frac{l}{\tau} & k \ge \frac{\alpha}{\alpha r (1+\beta) - r^2 \theta}. \end{cases}$$

$$(11)$$

The speed-density diagram is depicted in Fig. 6, which has distinct differences with its conventional variant for regular vehicles in which speed is non-increasing w.r.t. density. According to Fig. 6a, speed is constant at small densities (the threshold is presented in the panel with dashed lines), which is analogous to the free-flow speed of conventional vehicles. However, speed increases in mid-ranges of density due to cooperative sensing and increased sight. When density is large, speed decreases due to congestion. We also present a special case of the speed-density diagram in Fig. 6b, where $\beta = 0$ (non-cooperative sensing), resembling the case of disconnected CAVs. It is evident that Panel b is analogous to the conventional speed-density diagram with non-increasing speed.

2.4. Fundamental diagram

We now derive the fundamental diagram by defining the flow as a function of density. Let q denote vehicular flow on the corridor, derived from density and speed as q = kv. The fundamental diagram of restricted access corridors is depicted in Fig. 7. The surges in flow occur for the same reasons discussed in the speed-density relation. We also note that the fundamental diagram of restricted access corridors is a piece-wise linear function. This is consistent with Shi and Li (2021), which used trajectory data of commercial AVs to express the fundamental diagram.

We define the *capacity* as the maximum flow achievable denoted by $C(\alpha, \beta, \tau, \theta, r, l)$ (also defined by C for brevity) and given as

$$C = \max_{k} q(k), \tag{12}$$

where $k^{cr} = \arg \max_{k} q(k)$ is the critical density at which the capacity is achieved, and is equal to

$$k^{cr} = \frac{\alpha}{\alpha r(1+\beta) - r^2 \theta}.$$
(13)

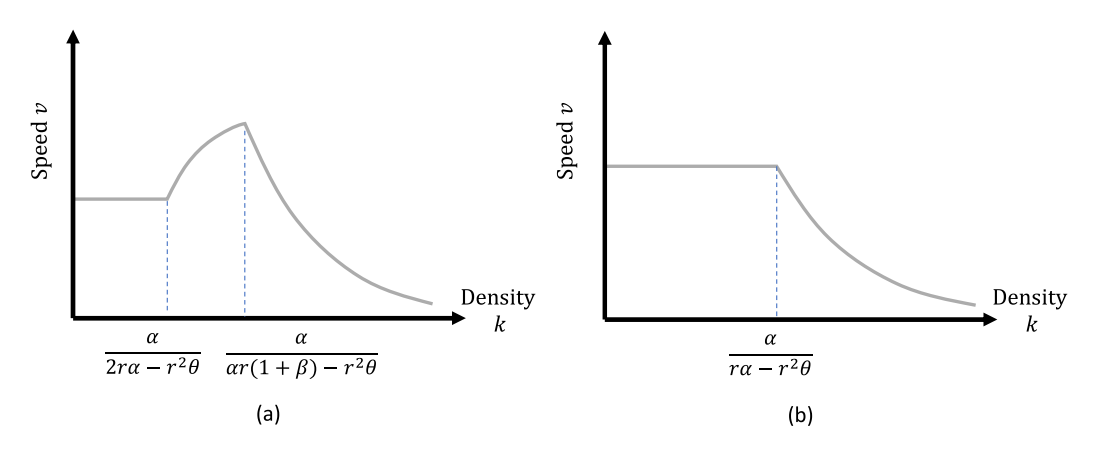


Fig. 6. (a) Speed-density profile, (b) non-cooperative ($\beta = 0$).

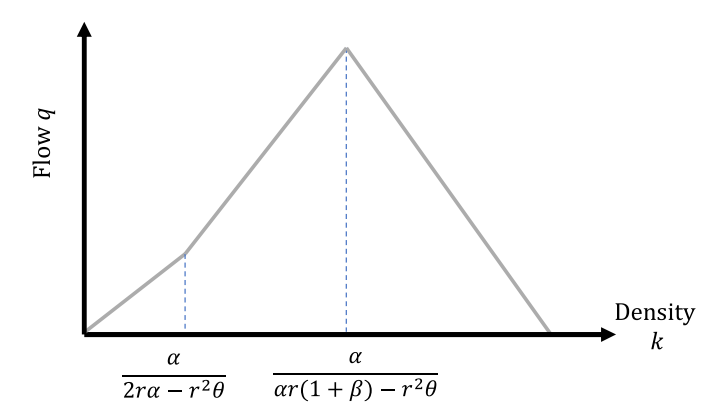


Fig. 7. Fundamental diagram of restricted access corridors.

Eq. (13) indicates that the critical density in restricted corridors always appears in uncongested conditions. Capacity is the flow achieved at the critical density, which is derived as

$$C = \frac{1}{\tau} - \frac{\alpha l}{\alpha r \tau (1+\beta) - r^2 \theta \tau}.$$
 (14)

We further discuss the impacts of sensor configuration and cooperative sensing below.

3. Optimal investment in individual vs. cooperative sensing

3.1. Capacity maximization

We assess the optimal investing of a limited budget in sensor power and/or the connectivity level. Improving sensor power may increase speed especially in no-overlap conditions, whereas improving connectivity can increase speed in the partial- and full-overlap conditions. We assume it costs c_{α} and c_{β} to manage and maintain one unit of sensor power or one unit of connectivity, respectively (Assumption 4). We define the total cost as $c_{\alpha}\alpha + c_{\beta}\beta$, which has to be lower than a given budget of B. We maximize capacity via the following mathematical model, where maximum capacity is obtained from (14).

$$\max_{\alpha,\beta} \frac{1}{\tau} - \frac{\alpha l}{\alpha r \tau (1+\beta) - r^2 \theta \tau}$$
s.t.
$$c_{\alpha} \alpha + c_{\beta} \beta \leq B,$$

$$\frac{\alpha}{r} \geq \theta,$$

$$r(1 - \frac{r\theta}{\alpha}) \geq l,$$

$$\alpha \geq 0,$$

$$0 \leq \beta \leq 1.$$
(15)

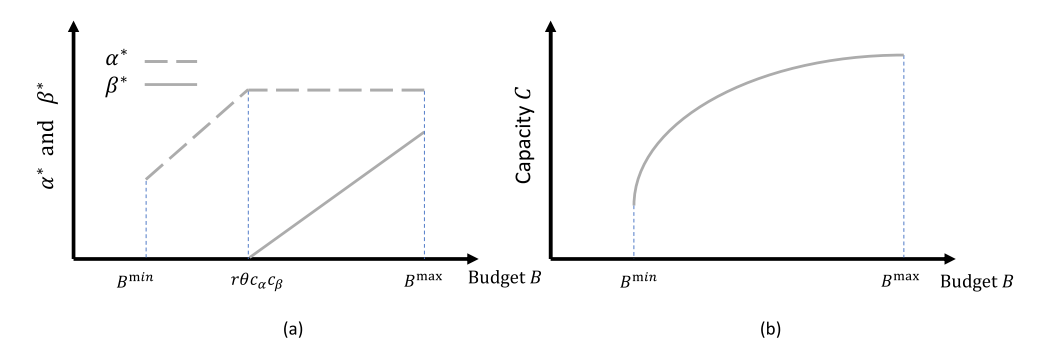


Fig. 8. (a) Optimal sensor power and connectivity ratio, (b) optimal capacity.

The first constraint is the budget condition; the second constraint ensures that the sensors have enough power to guarantee a non-negative speed in no-overlap travel conditions (see Fig. 4a); and the third constraint ensures a non-negative speed in no-overlap conditions which is derived from (10). The last two constraints state the limits of sensor power and connectivity level, respectively. The mathematical problem (15) is a nonlinear program with linear constraints. The objective function is also concave as shown in Appendix B.

We express the following insights from (15).

Lemma 1. The minimum required budget is

$$B^{\min} = \frac{r\theta c_a}{1 - I/r},\tag{16}$$

which is dedicated entirely to the sensor power.

According to (16), if $B < B^{\min}$ the budget is not large enough to maintain a sensor power for CAVs to adequately detect their surroundings and achieve a resolution larger than the safety threshold in no-overlap settings. In other words, (15) is infeasible for $B \le B^{\min}$. We present the optimal solution of (15) in the following lemma.

Lemma 2. The optimal sensor power and connectivity level are

$$(\alpha^*, \beta^*) = \begin{cases} (\frac{B}{c_{\alpha}}, 0) & B^{\min} \le B < \sqrt{r\theta c_{\alpha} c_{\beta}} \\ (\sqrt{\frac{r\theta c_{\beta}}{c_{\alpha}}}, \frac{B}{c_{\beta}} - \sqrt{\frac{r\theta c_{\alpha}}{c_{\beta}}}) & \sqrt{r\theta c_{\alpha} c_{\beta}} \le B. \end{cases}$$

$$(17)$$

According to Lemma 2, when the budget is lower than the defined threshold, $\sqrt{r\theta c_{\alpha} c_{\beta}}$, one should only invest in sensor power with the optimal value of $\alpha^* = B/c_{\alpha}$. In contrast, when the budget is larger than same threshold, second line of (17), part of the budget is also invested in connectivity. According to (17) the optimal sensor power and connectivity level, α^* and β^* , increase and decrease with range, respectively, because a larger range allows vehicles to become more independent in surveilling their surroundings, thus reducing the need for cooperative sensing.

We define the maximum budget, denoted by B^{max} , as the largest budget such that for any $B > B^{\text{max}}$ no improvement in capacity is achieved.

Lemma 3. The effective maximum budget for capacity maximization is

$$B^{\max} = c_{\beta} + \sqrt{r\theta c_{\alpha} c_{\beta}}.$$
 (18)

According to Lemma 2 and Eq. (18), we have full connectivity ($\beta = 1$) in restricted access corridors when the budget is B^{max} . Given Lemma 1–3 the profile of α^* and β^* are presented in Fig. 8a and the optimal capacity is depicted in Fig. 8b.

3.2. Social welfare maximization

We express the optimal sensor power and connectivity level chosen by a social planner that wants to maximize social welfare. Again, we assume travelers pay an amortized cost c_{α} and c_{β} for a unit of sensor power and connectivity, respectively. Moreover, we assume that the travelers experience a travel cost of c_t per unit of travel time t. Thus, the general cost for a traveler is $\mu = c_t t + c_\alpha \alpha + c_\beta \beta$. We focus on restricted access corridors and only consider the uncongested part of the fundamental diagram. Our intention is to assess pricing policies implemented to avoid undesirable congested traffic conditions that occur when density is larger than its critical (flow maximizing) threshold. In a similar spirit, the congested part of the fundamental diagram, which is experienced in

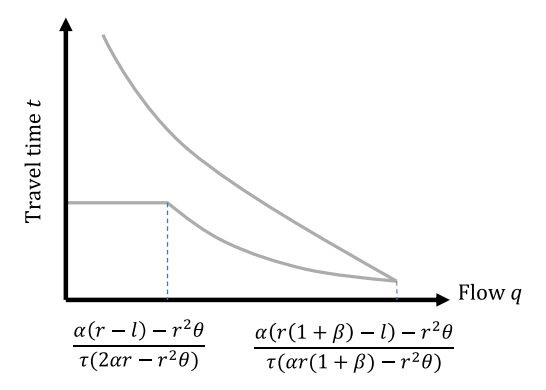


Fig. 9. Travel time of restricted access corridors.

cities such as Bangkok, Buenos Aires, and Mexico City (Hau, 2005) during peak hours, is not considered for planning purposes due to its inefficiency.

The expected travel time for a fixed corridor length, which we normalize to one, is $\frac{1}{n}$. Hence, using speed from (11), we have:

$$t = \begin{cases} \frac{\alpha \tau}{\alpha(r-l)-r^2\theta} & q \le \frac{\alpha(r-l)-r^2\theta}{\tau(2\alpha r - r^2\theta)} \\ \frac{(1-\beta)\alpha \tau}{(1+\beta)\alpha r - r^2\theta - \alpha l(1-\beta)} (1 + \frac{\beta}{(1-\beta)\tau q}) & \frac{\alpha(r-l)-r^2\theta}{\tau(2\alpha r - r^2\theta)} \le q \le \frac{\alpha(r(1+\beta)-l)-r^2\theta}{\tau(\alpha r(1+\beta)-r^2\theta)}, \end{cases}$$
(19)

which shows that travel time is non-increasing w.r.t. traffic flow for a given sensor power and connectivity level. Fig. 9 shows the travel time with respect to flow, which has a backward-bending part in congested traffic. Hence, for a given α and β , the travel time function is constant when q is below a threshold, and is decreasing with demand when q is above that threshold in the uncongested region. We call these the first and second leg of the travel time function, respectively.

The analysis period is considered to be a stretch of time during which the travel demand is only a function of the general cost. The demand is in CAVs per hour per lane and is denoted by $q = D(\mu)$. We consider the corridor's physical capacity to be fixed and equivalent to one lane. Therefore, any improvements in CAV throughput is achieved by investing in sensor power and/or connectivity level.

We present the social welfare maximization problem as

$$\max_{\alpha,\beta,q} W = \int_0^q D^{-1}(u)du - q(c_t t + c_\alpha \alpha + c_\beta \beta)$$
s.t. $\frac{\alpha}{r} \ge \theta$,
$$r(1 - \frac{r\theta}{\alpha}) \ge l,$$

$$\alpha \ge 0,$$

$$0 \le \beta \le 1,$$
(20)

where the first term of the objective function is the total willingness to pay and the second term is the total cost. The first two constraints ensure the sensor power is large enough for the CAVs to be moving for a given range, and the last two constraints state the ranges of sensor power and connectivity, respectively. The mathematical problem (20) is a nonlinear program with linear constraints. Thus, the presence of a unique and global solution relies on the concavity of the objective function that is the social welfare. We note that for a given α and β , the social welfare function is strictly concave w.r.t. demand q as long as the total willingness-to-pay function is strictly convex (Dixit et al., 1990). Global optimality w.r.t. all three variables, however, is not tractable due to the complexities of the travel time function. In the following analysis, we express the extreme points of the social welfare function and check local optimality by deriving the second derivative at that point numerically. We also discuss global optimality by comparing social welfare value at the obtained extreme points.

We consider the two legs of the travel time function individually. Travel time in the first leg depends neither on connectivity nor flow as expressed in (19). Therefore, we set connectivity to zero since it appears as a cost in social welfare. From the first-order condition, when in the first leg of travel time, setting $\frac{\partial W}{\partial q} = 0$ gives

$$D^{-1}(q) = c_t t + c_\alpha \alpha, \tag{21}$$

which shows that social welfare is maximized where the inverse demand and generalized cost functions intercept.

We now discuss the second leg of the travel time function. From the first-order condition, when in the second leg of travel time, setting $\frac{\partial W}{\partial q} = 0$ gives

$$D^{-1}(q) = (c_t t + c_\alpha \alpha + c_\beta \beta) + q c_t \frac{\partial t}{\partial a},\tag{22}$$

M. Nourinejad et al.

where

$$\frac{\partial t}{\partial q} = \frac{-\alpha \beta}{q^2 \left((1+\beta)\alpha r - r^2\theta - \alpha l(1-\beta) \right)}.$$
 (23)

Eq. (22) shows that social welfare is maximized where the inverse demand and marginal social cost functions (derivative of the second term of *W* w.r.t. *q*) intercept. Thus, the following proposition holds.

Lemma 4. Social welfare in sensor-equipped CAVs is maximized at demand q^* that is the intercept of the inverse demand function and the following step-wise marginal social cost function, denoted by Z, and given as

$$Z = \begin{cases} c_{\alpha}\alpha + \frac{c_{I}\alpha\tau}{\alpha(r-l)-r^{2}\theta} & q \leq \frac{\alpha(r-l)-r^{2}\theta}{\tau(2\alpha r-r^{2}\theta)} \\ c_{\beta}\beta + \alpha\left(c_{\alpha} + \frac{(1-\beta)c_{I}\tau}{\alpha\left(r(1+\beta)-l(1-\beta)\right)-r^{2}\theta}\right) & \frac{\alpha(r-l)-r^{2}\theta}{\tau(2\alpha r-r^{2}\theta)} \leq q \leq \frac{\alpha r(1+\beta)-r^{2}\theta-\alpha l}{\alpha\tau}. \end{cases}$$

$$(24)$$

Given Lemma 4, social welfare maximization is equivalent to social cost minimization in search of the optimal α^* and β^* . From the first-order condition, when in the first leg of social cost, setting $\frac{\partial Z}{\partial \alpha} = 0$ and $\frac{\partial Z}{\partial \beta} = 0$ give

$$\alpha^* = \frac{r^2 \theta}{r - l} + \frac{r}{r - l} \sqrt{\frac{\theta \tau c_t}{c_\alpha}},\tag{25}$$

$$\beta^* = 0. \tag{26}$$

From Lemma 4, any root finding algorithm can be used to find q^* at the intercept of the inverse demand function $D^{-1}(q)$ and the marginal social cost function in (24). We note that the intercept of $D^{-1}(q)$ with the first leg of Z has a closed-form solution of

$$q^* = D\left(\frac{(\sqrt{\tau c_t} + r\sqrt{\theta c_a})^2}{r - l}\right) \tag{27}$$

at the optimal α^* from (25).

Similarly, in the second leg of social cost from the first order condition, setting $\frac{\partial Z}{\partial a} = 0$ and $\frac{\partial Z}{\partial b} = 0$ give

$$\alpha^* = \frac{r}{r(1+\beta^*) - l(1-\beta^*)} \left(r\theta + \sqrt{\frac{(1-\beta^*)\theta\tau c_t}{c_\alpha}} \right),\tag{28}$$

$$\beta^* = \frac{1}{r+l} \left(\frac{r^2 \theta}{\alpha^*} - r + l + \sqrt{\frac{(2\alpha^* - r\theta)r\tau c_t}{\alpha^* c_{\beta}}} \right), \tag{29}$$

which is a system of two equations and two unknowns, α^* and β^* . Given the insensitivity of α^* and β^* w.r.t. q, the marginal social cost function, right side of (22), is also insensitive to q. The term $qc_l\frac{\partial t}{\partial q}$ is regarded as the road toll paid by drivers as a penalty for their contribution to social cost. In our setting, no road pricing is required in the first leg of travel time due to the uncongested status of the corridor. In the second leg, however, given that $\frac{\partial t}{\partial q} < 0$ from (23), the toll is actually a reward that is paid to travelers to encourage enough traffic flow for enhancing cooperative sensing amongst CAVs.

Fig. 10 shows the equilibrium point, denoted by e, where for a given α and β , the inverse demand function (dashed line) intersects the generalized cost function (solid line). Fig. 10(c) depicts the case where the two functions intersect both in the first and second legs of the travel time function. In this case there are two equilibrium points, e_1 and e_2 . The social welfare of the e_1 equilibrium is equal to the upper dashed area denoted by I, and the social welfare of the second equilibrium point, e_2 is equal to the area of both dashed areas (I and II). It is clear that in this case always the second point where the inverse demand and generalized cost function intersect in the second leg of travel time function provides a higher social welfare. We also note that it is possible that the inverse demand function intersects with the generalized cost function in the second leg of travel time function in two points. In such cases, again the point with higher flow provides higher social welfare.

4. Numerical findings

Our objectives from conducting the following numerical experiments are the following. We first present the impacts of the sensor configuration and connectivity level on traffic flow properties (sight, speed, and flow) at various traffic densities in Section 4.1. We then assess the properties of optimal social welfare maximizing policies and discuss the financial sustainability of the toll/reward, i.e., whether the investment in sensors and connectivity is paid off by the reward. Table 1 presents the default parameters of the numerical examples.

4.1. Connectivity properties

We assess the impacts of sensor configuration and connectivity on sight, speed, and flow at various CAV densities. The sight of the CAVs is affected by cooperative sensing as shown in Fig. 11. When $\beta = 0$ and CAVs are disconnected, or they are distant and

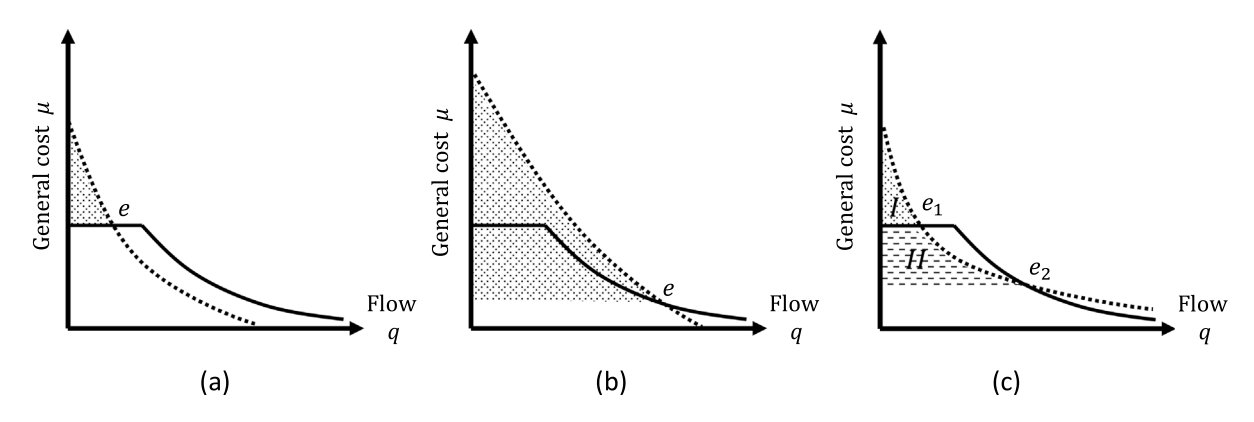


Fig. 10. Social welfare (dashed area) for different location where demand function (dashed line) intersects with the generalized cost (solid line).

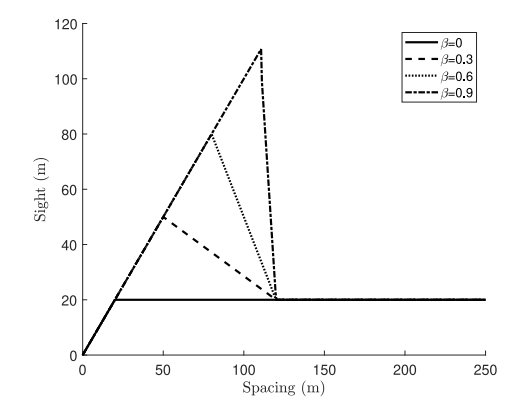


Fig. 11. Sight for different connectivity levels.

Table 1
Parameters of numerical examples.

Notation	Interpretation	Default value
α	Sensors' power	0.25 [data points]
1	Average length of vehicle	5 [m]
r	Sensors' range	100 [m]
θ	Safety threshold	$0.002 \left[\frac{\text{data point}}{m}\right]$
τ	Processing time	1 [s]

cannot share data, the sight is 20 m, which is considerably lower than sensors' range of 100 m. Nevertheless, the sight increases with the connectivity level when $\beta > 0$ in the mid-ranges of spacing (20–120 m), and can even exceed the range when $\beta = 0.9$.

Fig. 12 shows the speed-density profile for different sensor powers and connectivity levels. In the absence of connectivity, the free flow speed (at k=0) is 54 $\frac{km}{h}$ and 102 $\frac{km}{h}$ for sensor powers of $\alpha=0.25$ and $\alpha=0.3$, respectively. Moreover, the maximum speed increases with connectivity and can reach up to 200 $\frac{km}{h}$ with $\beta=0.5$ in both sensor power levels.

Fig. 13 shows the flow-density relation for different connectivity levels and sensor ranges. In the absence of connectivity, $\beta=0$, the maximum achievable capacity is 3000 $\frac{\text{veh}}{h}$ for 50 m range, which decreases to 2700 $\frac{\text{veh}}{h}$ for 100 m range. The drop in capacity at the larger range occurs because of the trade-off in resolution since the sensor power is fixed, see (1). One way of increasing capacity is to improve connectivity. The capacities increase to 3450 $\frac{\text{veh}}{h}$ and 3375 $\frac{\text{veh}}{h}$ for 50 m and 100 m sensor ranges, respectively, in full connectivity ($\beta=1$).

4.2. Optimal sensor power and connectivity level

We first assess the impacts of investing a limited budget in sensor power and/or connectivity level when maximizing corridor capacity. We assume that one unit of sensor power and connectivity costs \$0.5 and \$0.25, respectively, and we show the changes in optimal sensor power and connectivity in Fig. 14(a) and the capacity in Fig. 14(b) w.r.t. the budget. The minimum required sensor power is 0.2, and therefore, if the budget is less than \$0.1, the CAVs cannot satisfy the safety condition. Budgets less than \$0.16

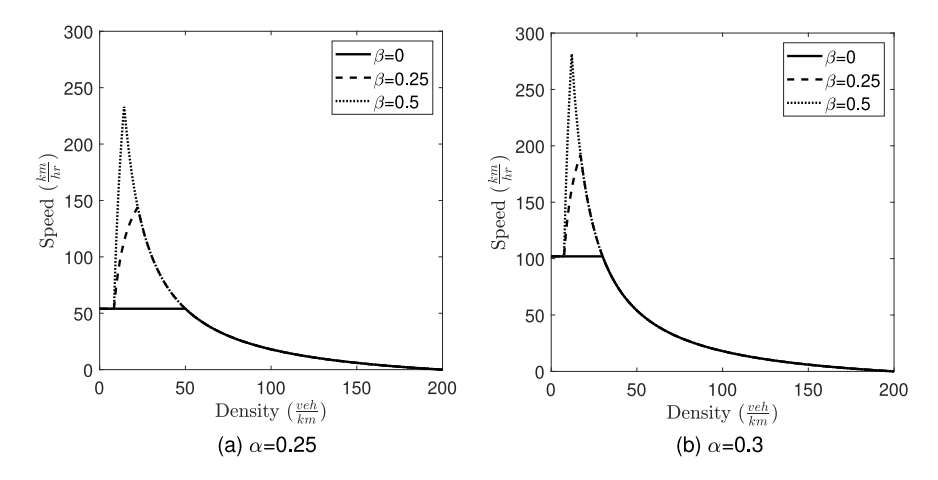


Fig. 12. Speed-density profile for different sensor powers and connectivity levels.

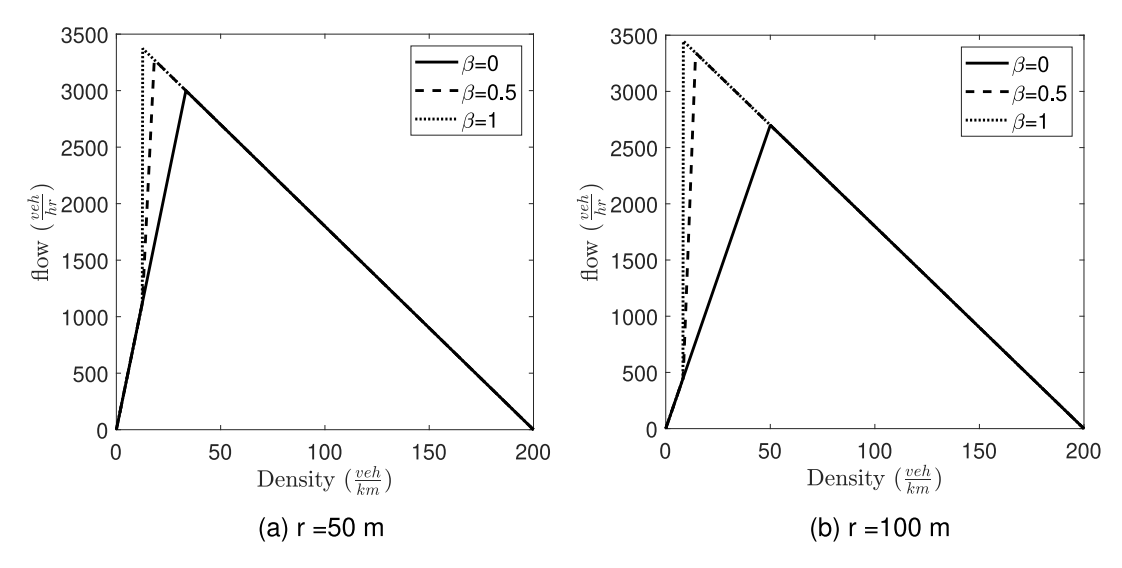


Fig. 13. Flow-density diagram for different sensor ranges and connectivity ratios.

are only invested in sensor power until the sensor power reaches $\alpha = 0.31$. Any more investments in sensor power is not optimal, and therefore the additional budget is invested in connectivity until $\beta = 1$, at which the maximum capacity is 3470 $\frac{\text{veh}}{\text{h}}$.

Moreover, we vary the marginal sensor and connectivity costs c_{α} and c_{β} , and present the minimum and maximum required budget changes in Fig. 15. We observe that the required minimum budget is insensitive to the connectivity cost and changes only with the sensor power cost. This happens as the CAVs need some level of sensor power to be able to drive safely relying solely on their own sensor data. In contrast, the maximum required budget changes with both marginal sensor and connectivity costs. The maximum required budget is more sensitive to the connectivity cost, since the CAVs stretch of vision can only be extended by cooperative sensing through connectivity beyond a threshold in density.

We investigate social welfare maximizing policies when adjusting sensor power and the connectivity level. The processing time is $\tau=1$, travelers experience a marginal travel cost of $c_t=10\,\frac{5}{h}$, and demand is $q=exp(-\mu)$ where μ is the generalized cost. We vary the marginal sensor power and connectivity costs, c_α and c_β , and used Newton root finding algorithm to find the optimal sensor power, connectivity, and social welfare presented in Fig. 16, which has the following patterns.

Complimentary configurations: Fig. 16a-b shows that when the marginal connectivity cost is high, the social planner only invests in sensor power. In contrast, when the sensor power cost is high, the social planner invests more on connectivity to benefit from cooperative sensing while ensuring the minimum sensor power is in place.

Ineffective connectivity: The black colored area in Fig. 16b encloses the set of costs where the social planner does not invest in connectivity due to its higher cost over benefit to congestion alleviation. This area represents cases where the inverse demand function intercepts the first leg of the social cost function, indicating the demand is not sufficient enough to reach density levels that can leverage the benefits of cooperative sensing.

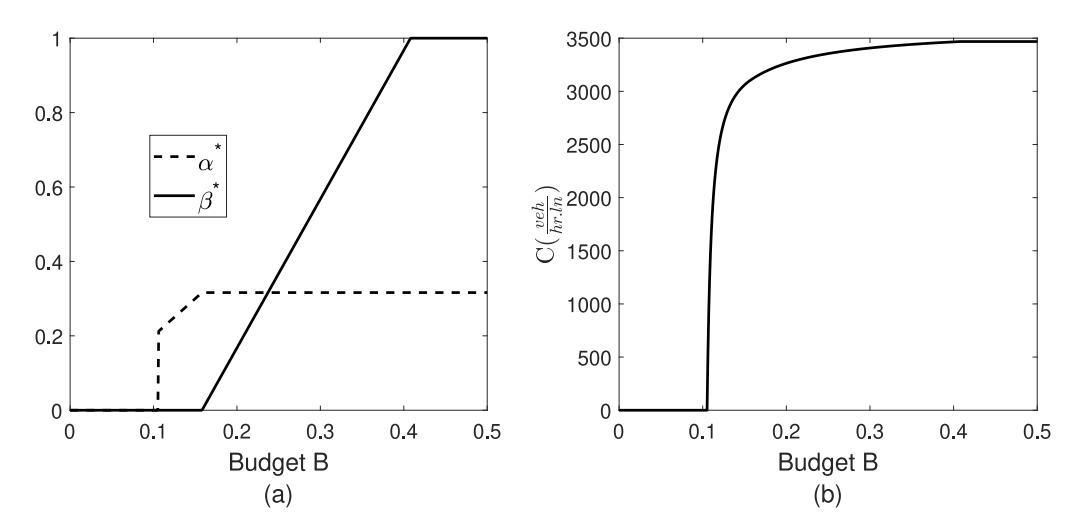


Fig. 14. (a) Optimal sensor power and connectivity level; (b) optimal capacity.

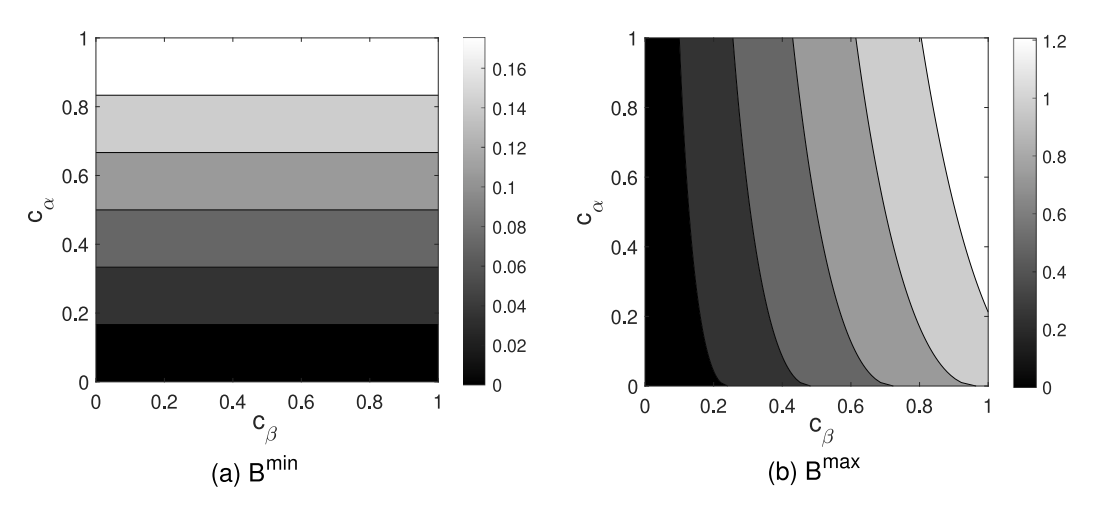


Fig. 15. Changes in (a) minimum budget, and (b) maximum budget w.r.t. costs of sensor power and connectivity.

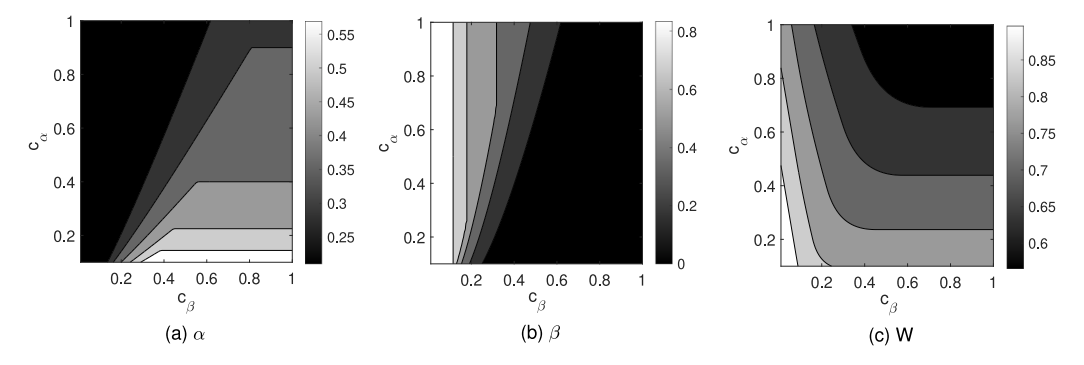


Fig. 16. Changes in (a) optimal sensor power, (b) connectivity level, and (c) social welfare w.r.t. costs of sensor power and connectivity.

Social welfare trends: Fig. 16c presents social welfare, which decreases with the marginal costs of sensor power and connectivity. We present in Fig. 17: (a) the toll charged by the social planner to each traveler, $qc_1\frac{\partial t}{\partial q}$; (b) the traveler out-of-pocket cost, $c_\alpha\alpha + c_\beta\beta$; and (c) the summation of the first two, which can be positive indicating the surplus is a payment from travelers to the social planner, or negative indicating that the surplus is a reward from the social planner to travelers. Fig. 17(a) shows that when the connectivity cost is high, no toll is needed, and no reward is paid. However, when the connectivity cost is low, a toll is

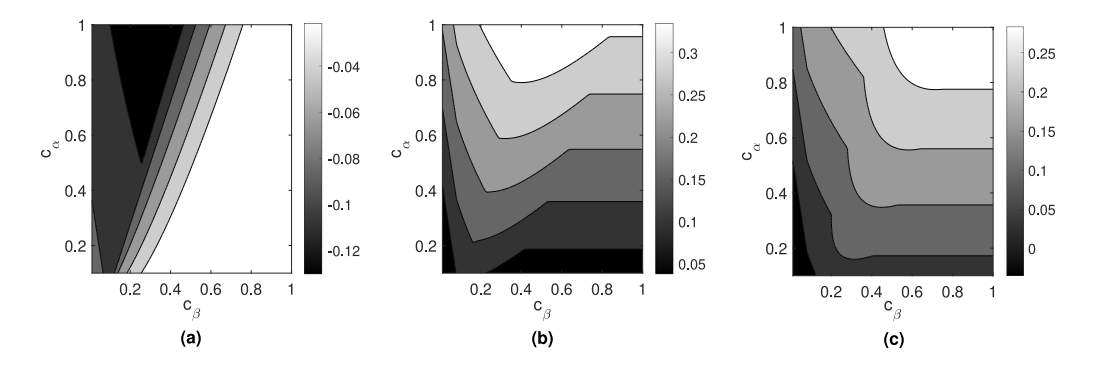


Fig. 17. Changes in optimal (a) toll $(qc_i\frac{dt}{\partial a})$, (b) travelers out-of-pocket cost $(c_a\alpha + c_\beta\beta)$, and (c) their summation w.r.t. costs of sensor power and connectivity.

needed, which is negative and works as a reward to be paid to travelers to encourage the cooperative sensing. Fig. 17(c) shows that when the costs of sensor power and connectivity are low, the reward is higher than the travelers out-of-pocket cost, but it becomes economically sustainable with an increase in either sensor power or connectivity cost.

5. Conclusions and future research

CAVs rely on their sensors to detect their surroundings and drive safely. Sharing sensor data with other nearby CAVs is a cooperative strategy that can improve safety and efficiency, since each CAV retains a richer vision of its surroundings. This study investigates how individual and cooperative sensing can impact automated driving to facilitate policy discussion on CAVs sensor configuration and connectivity. We present a stylized model of CAV mobility, showing that there exists a threshold density beyond which the sensors of two adjacent CAVs have sufficient overlap in their detection range to facilitate cooperative sensing, thereby allowing vehicles to drive at faster speeds due to their enhanced vision of their surroundings. We then investigate the short- and long-term impacts of investing in either sensors or connectivity amongst CAVs. According to the analysis, investing in corridor capacity should be disjoint, first prioritizing sensor power so the CAVs can drive independently in low density traffic, and then investing in CAV connectivity to enhance vision at medium density traffic. In terms of pricing, social welfare analysis shows that travelers should be granted a reward, which increases the density of CAVs and enables cooperative sensing amongst them.

Future research can consider the impacts of highway infrastructure, such as roadside units in modeling cooperative sensing and extend the connectivity from vehicle-to-vehicle to vehicle-to-infrastructure. This type of analysis would also yield a better understanding of the trade-offs between stationary (roadside) and moving (on board vehicle) sensors. The former has full temporal coverage of a limited space within the sensor's range, whereas the latter has partial temporal coverage of a much larger area since the CAVs gather information from the entire network. Moreover, while this study focused only on the information sharing between vehicles following each other in the same lane, the possibility of sharing information with vehicles moving in adjacent lanes or in the opposite direction is worth investigating. Lastly, we consider the uniform distribution of vehicles along the corridor in deriving the fundamental diagrams in this study. In future studies, it is worth investigating the randomness of vehicles spacing along the corridors.

Acknowledgments

The work described in this paper was partly supported by research grants from the National Science Foundation, United States (CMMI-1904575).

Appendix A

We consider unrestricted access corridors open to other road users, such as pedestrians, and indicating that the vehicles may encounter stationary objects on the road. A rural highway or an urban street is an example of such a traffic corridor. Consider an unrestricted corridor where a stationary object may appear on the road. Using Kinematics, and given that the ego vehicle's speed drops from v to zero within distance T - l from the object, the safe speed is set as

$$v = \sqrt{(a\tau)^2 + 2a(T-l)} - a\tau,$$
 (30)

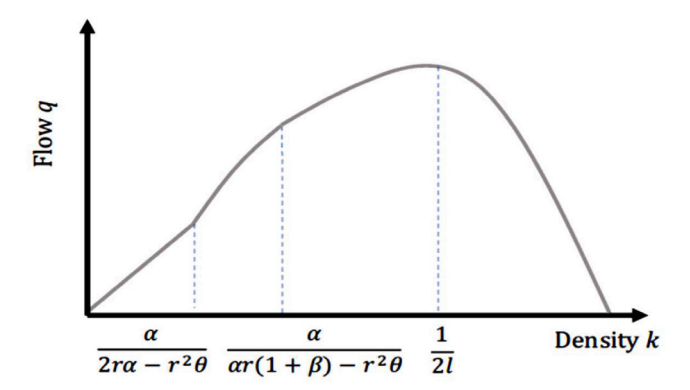


Fig. 18. Fundamental diagram of unrestricted access corridors.

where a is the braking deceleration, and τ is the processing time of CAVs. Similarly, we can discuss the speed-density relationship. Speed for a given density k using Eq. (10) is

$$v = \begin{cases} \sqrt{(a\tau)^2 + 2a(r - \frac{r^2\theta}{\alpha} - l)} - a\tau & k < \frac{\alpha}{2\alpha r - r^2\theta} \\ \sqrt{(a\tau)^2 + 2a(\frac{(1+\beta)r}{1-\beta} - \frac{\beta}{(1-\beta)k} - \frac{r^2\theta}{(1-\beta)\alpha} - l)} - a\tau & \frac{\alpha}{2\alpha r - r^2\theta} \le k < \frac{\alpha}{\alpha r (1+\beta) - r^2\theta} \\ \sqrt{(a\tau)^2 + 2a(\frac{1}{k} - l)} - a\tau & k \ge \frac{\alpha}{\alpha r (1+\beta) - r^2\theta} \end{cases}$$
(31)

The speed-density diagram of unrestricted access corridors has the same general shape as restricted access corridors depicted in Fig. 6, and the only difference is in the maximum achievable speed.

We derive the fundamental diagram from flow q = kv. The fundamental diagram of unrestricted access corridors is depicted in Fig. 18, which is analogous to the conventional fundamental diagram.

We can now derive the critical density for unrestricted access corridors as

$$k^{cr} = \max\{\frac{\alpha}{\alpha r(1+\theta) - r^2\theta}, \frac{1}{2l}\}.$$
(32)

Eq. (32) indicates that the critical density in unrestricted access corridors occurs either in congested conditions with a sight of s and critical density 1/2l, or in uncongested conditions with the sight larger than s. Thus, capacity, which is the flow achieved at the critical density, is derived as:

$$C = \begin{cases} \frac{\alpha}{\alpha r(1+\beta) - r^2 \theta} \left(\sqrt{(a\tau)^2 + 2a(\frac{\alpha r(1+\beta) - r^2 \theta}{\alpha} - l)} - a\tau \right) & l \ge \frac{\alpha r(1+\beta) - r^2 \theta}{2\alpha} \\ \frac{\sqrt{(a\tau)^2 + 2al - a\tau}}{2l} & l < \frac{\alpha r(1+\beta) - r^2 \theta}{2\alpha} \end{cases}$$
(33)

Using (15) to maximize the capacity of unrestricted access corridors yields the same minimum budget as restricted corridors presented in Lemma 1, and optimal values of sensor power and connectivity as presented in Lemma 2. However, the maximum budget for unrestricted corridors is

$$B^{\max} = 2\sqrt{r\theta c_{\alpha}c_{\beta}} - c_{\beta}(1 - \frac{2l}{r}). \tag{34}$$

According to Eq. (34), at $B = B^{\max}$ the critical density is $k_{cr} = 1/2l$, which indicates that traffic flow is impeded by the large number of vehicles on the corridor and not by the sensor power and connectivity. Therefore, any investment above B^{\max} does not improve capacity in unrestricted corridors.

Appendix B

Proof. The Hessian of the objective function is

$$\begin{bmatrix} -\frac{2l\theta(1+\beta)}{\tau(\alpha(1+\beta)-r\theta)^3} & -\frac{2l\theta\alpha}{\tau(\alpha(1+\beta)-r\theta)^3} \\ -\frac{2l\theta\alpha}{\tau(\alpha(1+\beta)-r\theta)^3} & -\frac{2l\alpha^3}{r\tau(\alpha(1+\beta)-r\theta)^3} \end{bmatrix},$$

and its eigenvalues are equal to

$$-\frac{l\bigg(\alpha^3+r\theta(1+\beta)+\sqrt{\alpha^3+r\theta(1+\beta)-4\alpha^2r\theta(\alpha(1+\beta)-r\theta)}\bigg)}{r\tau\bigg(\alpha(1+\beta)-r\theta\bigg)^3},$$

$$\frac{l \left(\alpha^3 + r\theta(1+\beta) - \sqrt{\alpha^3 + r\theta(1+\beta) - 4\alpha^2 r\theta(\alpha(1+\beta) - r\theta)}\right)}{r\tau \left(\alpha(1+\beta) - r\theta\right)^3}$$

It is obvious that the nominators are positive. Moreover, we have $\alpha \ge r\theta$ from the second constraint, and the denominators are positive. Thus, the eigenvalues of the Hessian matrix are negative and the Hessian matrix is negative definite. Therefore, the objective function is concave, and there exists a global optimum solution. \Box

Appendix C

Nomenclature

- A Augmented resolution
- a Acceleration rate
- B Budget
- C Capacity
- c_{α} Cost to manage and maintain one unit of sensor power
- c_{β} Cost to manage and maintain one unit of connectivity
- c_t Travel cost per unit of travel time
- D Travel demand function
- d Deceleration rate
- k Density
- *k*^{cr} Critical density
- 1 Safety distance
- q Flow
- R Resolution
- r Range
- s Spacing between the leader and ego vehicle
- T Sensor's sight
- t Travel time
- v Speed
- W Social welfare
- x Distance from ego vehicle
- Z Social cost
- α Sensor's power
- β Connectivity ratio
- θ Safety threshold parameter
- μ Traveler general cost
- *τ* Processing time

References

Campolo, C., Molinaro, A., Iera, A., Menichella, F., 2017. 5G network slicing for vehicle-to-everything services. IEEE Wirel. Commun. 24 (6), 38–45.

Dixit, A.K., Sherrerd, J.J., et al., 1990. Optimization in Economic Theory. Oxford University Press on Demand.

Fedorov, I., Lawal, N., O'Nils, M., Alqaysi, H., 2017. Placement strategy of multi-camera volumetric surveillance system for activities monitoring. In: Proceedings of the 11th International Conference on Distributed Smart Cameras. pp. 113–118.

Ha, P., Chen, S., Du, R., Dong, J., Li, Y., Labi, S., 2020. Vehicle connectivity and automation: a sibling relationship. Front. Built Environ. 199.

Hall, D., Llinas, J., 2001. Multisensor Data Fusion. CRC Press.

Hau, T.D., 2005. Economic fundamentals of road pricing: a diagrammatic analysis, Part I-Fundamentals. Transportmetrica 1 (2), 81-117.

Kianfar, R., Augusto, B., Ebadighajari, A., Hakeem, U., Nilsson, J., Raza, A., Tabar, R.S., Irukulapati, N.V., Englund, C., Falcone, P., et al., 2012. Design and experimental validation of a cooperative driving system in the grand cooperative driving challenge. IEEE Trans. Intell. Transp. Syst. 13 (3), 994–1007.

Labi, S., 2021. Measuring the benefits of civil systems connectivity and automation-a discussion in the context of highway transport. Civ. Eng. Environ. Syst. 1-21

Rinner, B., Quaritsch, M., 2009. Embedded middleware for smart camera networks and sensor fusion.

Shi, X., Li, X., 2021. Constructing a fundamental diagram for traffic flow with automated vehicles: Methodology and demonstration. Transp. Res. B 150, 279–292. Theia Technologies, 2022. How to calculate image resolution. URL https://static1.squarespace.com/static/551ecflae4b0b101cf72bfa3/t/55412684e4b0512f43caa5de/1430333060072/Resolution_calculation.pdf.

Vignon, D.A., Yin, Y., Bahrami, S., Laberteaux, K., 2022. Economic analysis of vehicle infrastructure cooperation for driving automation. Transportation Research Part C: Emerging Technologies 142, 103757.

Visser, A., Groen, F., 1999. Organisation and design of autonomous systems. Textbook, faculty of mathematics. In: Computer Science, Physics and Astronomy. vol. 403, University of Amsterdam, Kruislaan.

Wang, M., Daamen, W., Hoogendoorn, S.P., van Arem, B., 2014a. Rolling horizon control framework for driver assistance systems. Part I: Mathematical formulation and non-cooperative systems. Transp. Res. C 40, 271–289.

Wang, M., Daamen, W., Hoogendoorn, S.P., van Arem, B., 2014b. Rolling horizon control framework for driver assistance systems. Part II: Cooperative sensing and cooperative control. Transp. Res. C 40, 290–311.

Wang, C., Gong, S., Zhou, A., Li, T., Peeta, S., 2020. Cooperative adaptive cruise control for connected autonomous vehicles by factoring communication-related constraints. Transp. Res. C 113, 124–145.

Yeong, D.J., Velasco-Hernandez, G., Barry, J., Walsh, J., et al., 2021. Sensor and sensor fusion technology in autonomous vehicles: A review. Sensors 21 (6), 2140.

Zeadally, S., Javed, M.A., Hamida, E.B., 2020. Vehicular communications for ITS: standardization and challenges. IEEE Commun. Stand. Mag. 4 (1), 11-17.